

Bandgap Tailored Nonfullerene Acceptors for Low Energy Loss Near-Infrared Organic Photovoltaics

Jaewon Lee, Seyeong Song, Jianfei Huang, Zhifang Du, Hansol Lee, Ziyue Zhu, Seo-Jin Ko, Thuc-Quyen Nguyen, Jin Young Kim, Kilwon Cho, and Guillermo C. Bazan

ACS Materials Lett., **Just Accepted Manuscript** • DOI: 10.1021/acsmaterialslett.9b00512 • Publication Date (Web): 06 Mar 2020

Downloaded from pubs.acs.org on March 9, 2020

Just Accepted

“Just Accepted” manuscripts have been peer-reviewed and accepted for publication. They are posted online prior to technical editing, formatting for publication and author proofing. The American Chemical Society provides “Just Accepted” as a service to the research community to expedite the dissemination of scientific material as soon as possible after acceptance. “Just Accepted” manuscripts appear in full in PDF format accompanied by an HTML abstract. “Just Accepted” manuscripts have been fully peer reviewed, but should not be considered the official version of record. They are citable by the Digital Object Identifier (DOI®). “Just Accepted” is an optional service offered to authors. Therefore, the “Just Accepted” Web site may not include all articles that will be published in the journal. After a manuscript is technically edited and formatted, it will be removed from the “Just Accepted” Web site and published as an ASAP article. Note that technical editing may introduce minor changes to the manuscript text and/or graphics which could affect content, and all legal disclaimers and ethical guidelines that apply to the journal pertain. ACS cannot be held responsible for errors or consequences arising from the use of information contained in these “Just Accepted” manuscripts.

Bandgap Tailored Nonfullerene Acceptors for Low Energy Loss Near-Infrared Organic Photovoltaics

Jaewon Lee,^{†,‡,¥} Seyeong Song,^{†,§} Jianfei Huang,[†] Zhifang Du,[†] Hansol Lee,[‡] Ziyue Zhu,[†] Seo-Jin Ko,^{||} Thuc-Quyen Nguyen,[†] Jin Young Kim,[§] Kilwon Cho,^{*,‡} Guillermo C. Bazan^{*,†}

[†]Center for Polymers and Organic Solids, Departments of Chemistry and Biochemistry, University of California at Santa Barbara, Santa Barbara, California 93106, United States

[‡]Center for Advanced Soft Electronics, Department of Chemical Engineering, Pohang University of Science and Technology, Pohang, 37673, Republic of Korea

[§]Department of Energy Engineering, Ulsan National Institute of Science and Technology, Ulsan 44919, Republic of Korea

^{||}Division of Advanced Materials, Korea Research Institute of Chemical Technology, Daejeon 34114, Republic of Korea

[¥]Present address: Department of Chemical Engineering and Applied Chemistry, Chungnam National University, Daejeon, 34134, Republic of Korea

ABSTRACT: A series of A- π -D- π -A type nonfullerene acceptors (NFAs) was designed and synthesized with the goal of optimizing light absorption and energy losses in near-infrared (NIR) organic solar cells (OSCs) principally through the use of side chain engineering. Specific molecules include p-IO1, o-IO1, p-IO2, and o-IO2 with optical bandgaps of 1.34 eV, 1.28 eV, 1.24 eV, and 1.20 eV, respectively. Manipulating the optoelectronic properties and intermolecular organization by substituting bulky phenylhexyl (p-) for linear octyl chains (o-) and replacing bisalkoxy (-O2) with alkyl-alkoxy combination (-O1) allows one to target energy bandgaps and achieve a favorable bulk heterojunction morphology when in the presence of the donor polymer PTB7-Th. Solar cells based on o-IO1 and PTB7-Th exhibit an optimal power conversion efficiency of 13.1%. The excellent photovoltaic performance obtained with the o-IO1 acceptor can be attributed to a short-circuit current of 26.3 mA cm⁻² and energy losses on the order of 0.54 eV. These results further highlight how side chain engineering is a straightforward strategy to tune the molecular design of n-type molecular semiconductors, particularly in the context of near-infrared high efficiency organic photovoltaics.

Organic semiconductors are characterized by a broad structural diversity that allows fine tuning of optical bandgaps and orbital energy levels, and the ability to be processed into thin, light-weight, and flexible devices.¹⁻⁵ Near-infrared (NIR) responsive organic semiconductors have the potential for integration into building windows, greenhouse rooftops, and automobile glass as semitransparent energy generating modules,⁶⁻⁹ as well as optical sensors for health monitoring, image sensing, and night surveillance.¹⁰⁻¹² Rational design of high performance organic semiconductors with NIR absorption capabilities in bulk heterojunction (BHJ) organic solar cells (OSCs) provides interesting challenges,¹³⁻¹⁵ and in particular how to best accommodate the inherent trade-off between the driving force for charge separation and voltage loss in the device.¹⁶⁻²⁰ Careful consideration must be given to the frontier molecular orbitals and energetic offsets in the components of the BHJ blend to efficiently dissociate photo-generated excitons and achieve the highest possible open-circuit voltage (V_{OC}).²¹⁻²³

Nonfullerene acceptors (NFAs) with NIR absorption for BHJ blends have attracted recent interest.²⁴⁻²⁶ They benefit from the structural diversity offered by multiple combinations of ladder-type central donor (electron rich) and acceptor (electron poor) end groups; this feature has endowed acceptor-donor-acceptor (A-D-A) type NFAs with narrow bandgap properties and provided energetics suitable for NIR solar cell fabrication.²⁷⁻³⁰ NFAs with ultra-narrow bandgap (UNBG) properties (defined arbitrarily as $E_g^{opt} \leq 1.3$ eV) have also been successfully designed.³¹⁻³⁶ Of note is that the design of UNBG-NFAs has led

to short-circuit current densities (J_{SC}) of over 20 mA cm⁻² due in part to a broad photoresponse in the NIR region. Incorporating π -bridge units to form an A- π -D- π -A configuration provides further opportunities to optimize intramolecular charge transfer (ICT) characteristics, energy levels, and BHJ morphology.^{32,37-39} It is also encouraging that driving energies for efficient charge separation in NFA solar cells are smaller than empirical 0.3 eV observed in fullerene-based OSCs,⁴⁰⁻⁴⁴ which is advantageous to minimize energy losses from the difference between optical bandgap (E_g^{opt}) and V_{OC} of the solar cell device ($E_{loss} = E_g^{opt} - eV_{OC}$); this enables high photocurrents and high

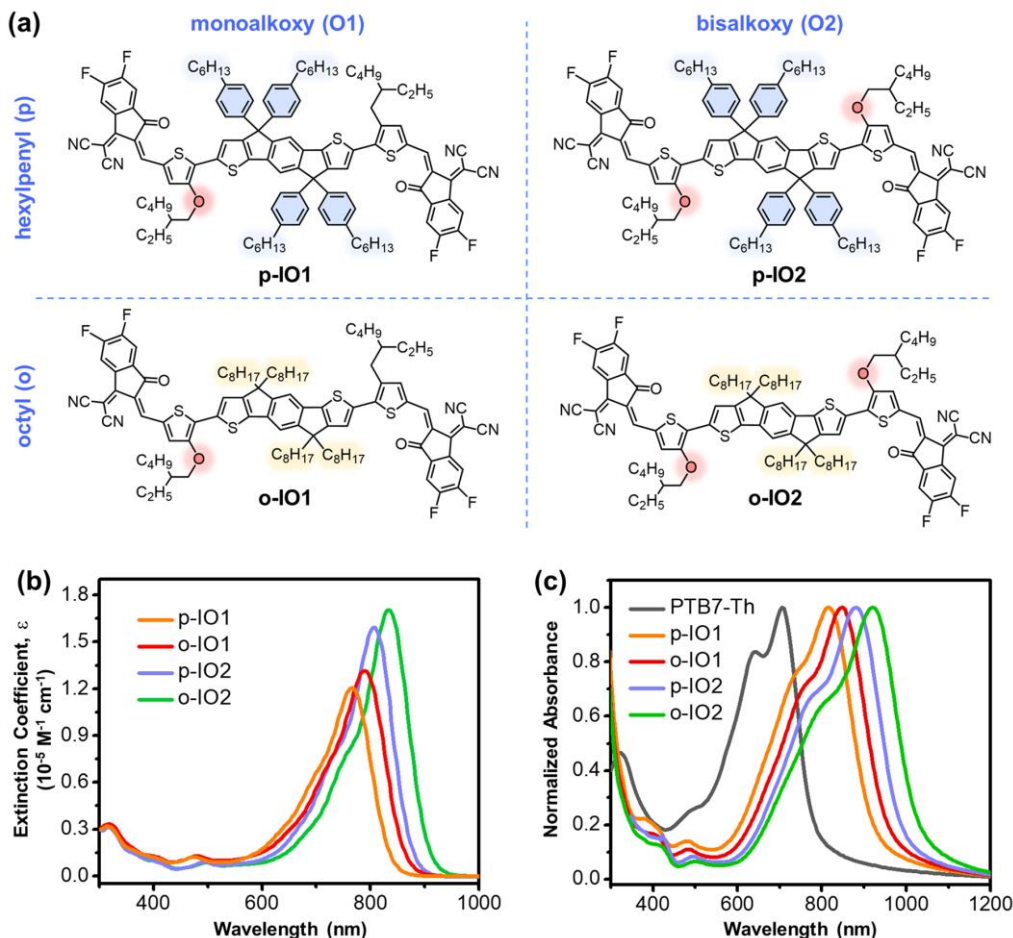


Figure 1. (a) Molecular structures of p-IO1, o-IO1, p-IO2, and o-IO2. Absorption spectra of (b) solution in chloroform and (c) thin films.

voltage to be achieved simultaneously, particularly in UNBG heterojunctions.^{22,34}

In this contribution, we disclose a series of A- π -D- π -A type NFAs with UNBG properties for use in NIR solar cell applications. Our molecular design includes structural variations through side chain engineering for the purpose of tuning desirable properties. Consequently, p-IO1, o-IO1, p-IO2, and o-IO2 are constructed based on an indaceno[1,2-*b*:5,6-*b'*]dithiophene (IDT) central donor core (D), thienyl π -bridges (π), and 1,1-dicyanomethylene-5,6-difluoro-3-indanone terminal acceptors (A), see **Figure 1**. These molecules possess identical conjugated framework skeletons, but differ with respect to the solubilizing side chains, specifically alkyl vs. alkoxy on the π -bridges and octyl vs. 4-hexylphenyl on the D core. One finds that replacing bulky hexylphenyl chains (p-IO2 and p-IO1) with linear octyl chains (o-IO2 and o-IO1) on the D core leads to improved packing ability and decreases the optical bandgap. By changing the number of alkoxy groups on the thienyl π -bridges, one can modulate intramolecular charge transfer (ICT) characteristics. Devices fabricated using the non-symmetric o-IO1, which bears linear octyl chains on the IDT central core and alkyl and alkoxy chains on the thienyl π -bridges, in combination with the donor conjugated polymer PTB7-Th are able to achieve a

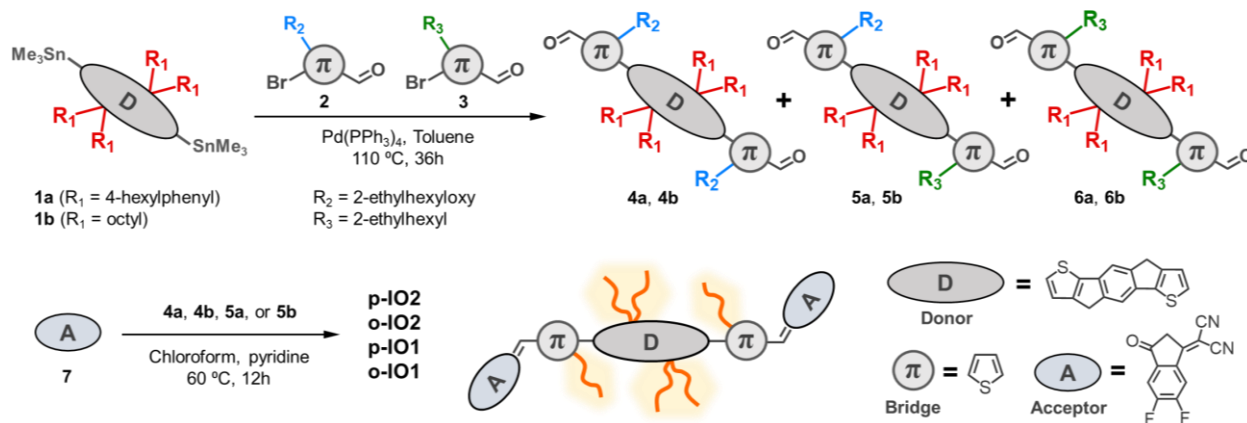
power conversion efficiency PCE of 13.1% with a short circuit current (J_{SC}) of 26.3 mA cm⁻² and $E_{loss} = 0.54$ eV.

Synthetic routes for the preparations of p-IO1, o-IO1, p-IO2, and o-IO2 are provided in **Scheme 1**. The key intermediates (4a, 4b, 5a, and 5b) were synthesized by Stille coupling of

Table 1. Optical properties and estimates of frontier energy levels of PTB7-Th, p-IO1, o-IO1, p-IO2, and o-IO2.

compound	$\lambda_{f,max}$ (nm) ^a	$\lambda_{f,max}$ (nm) ^b	E_g^{opt} (eV) ^c	HOMO (eV) ^d	LUMO (eV) ^e
PTB7-Th	-	705	1.58	-5.20	-3.46
p-IO1	766	815	1.34	-5.46	-4.13
o-IO1	790	850	1.28	-5.44	-4.15
p-IO2	808	880	1.24	-5.44	-4.19
o-IO2	835	920	1.20	-5.41	-4.21

^aAbsorption maximum in solution. ^bAbsorption maximum in thin film. ^cOptical bandgap calculated from the absorption edge of the thin film. ^dHOMO energy level estimated from the oxidation onset. ^eLUMO energy level estimated from the potential of the reduction onset.



Scheme 1. Synthetic procedure for the preparations of p-IO2, o-IO2, p-IO1, and o-IO1.

bis(stanny)l IDT (**1a** or **1b**) and monobromo thienyl π -bridges with alkyl and alkoxy side chains (**2** and **3**). Knoevenagel condensation of dialdehyde precursors (**4a**, **4b**, **5a**, and **5b**) with 1,1-dicyanomethylene-5,6-difluoro-3-indanone afforded the target NFAs: p-IO1, o-IO1, p-IO2, and o-IO2 in yields of >80%. All new compounds and intermediates were characterized by conventional methods (see Supporting Information, Figures S1–S8).

The optical absorption spectra of p-IO2, p-IO1, o-IO2, and o-IO1 in dilute chloroform solutions are provided in Figure 1b. One observes that the absorption maximum (λ_{\max}) red-shifts gradually from 766 nm (p-IO1) to 790 nm (o-IO1) to 808 nm (p-IO2), and then to 835 nm (o-IO2); the λ_{\max} red-shifts approximately ~25 nm by replacing bulky phenylhexyl with linear octyl chains on D and ~45 nm by replacing alkyl with alkoxy chains on π , respectively. The molar extinction coefficient (ϵ_{\max}) of o-IO1 was calculated to be $1.32 \times 10^5 \text{ M}^{-1} \text{ cm}^{-1}$, which is slightly larger than that of p-IO1 ($1.20 \times 10^5 \text{ M}^{-1} \text{ cm}^{-1}$). A similar trend was observed with their analogues: o-IO2 vs. p-IO2 ($1.70 \times 10^5 \text{ M}^{-1} \text{ cm}^{-1}$ vs. $1.59 \times 10^5 \text{ M}^{-1} \text{ cm}^{-1}$). From the UV–vis–NIR absorption spectra of NFAs as thin films shown in Figure 1c and Figure S9, one observes absorption capabilities in the range of 600–1050 nm, with the maxima located at 815, 850, 880, and 920 nm for p-IO1, o-IO1, p-IO2, and o-IO2, respectively. The red-shifted wavelengths from solution to thin films are approximately 49 nm, 60 nm, 72 nm, and 85 nm for p-IO1, o-IO1, p-IO2, and o-IO2, respectively, leading to optical bandgaps of 1.34 eV (p-IO1), 1.28 eV (o-IO1), 1.24 eV (p-IO2), and 1.20 eV (o-IO2) as determined from the onset of film absorption according to the relationship $E_g^{\text{opt}} = 1240/\lambda_{\text{edge}}$. One concludes from these comparative studies that incorporating linear octyl instead of bulky phenylhexyl side chains leads to a red-shifted λ_{\max} . For instance, compare the λ_{\max} of o-IO2 (920 nm) vs. p-IO2 (880 nm). Replacing alkoxy side chains with alkyl side chains at the thienyl π -bridges leads to a blue-shifted λ_{\max} (o-IO2 (920 nm) vs. o-IO1 (850 nm)), most likely due to a reduction in the electron density in the interior of the molecular skeleton and concomitant weakening of the intramolecular charge transfer (ICT). From a practical perspective, it is worth

noting the complementary absorption spectra and orbital energy levels between the NFAs and PTB7-Th for achieving broad absorption of sunlight (Table 1). Highest occupied molecular orbital (HOMO) and lowest unoccupied molecular orbital (LUMO) levels were estimated by using cyclic voltammetry (Table 1), and their cyclic voltammograms are shown in Figure S10. Altogether, the optical absorption and molecular orbital level results provide the framework to appreciate the degree to which permuting the side chains can be used to modulate the optoelectronic properties built within this specific conjugated ICT core.

Solar cells with the inverted device structure comprising ITO/ZnO/PTB7-Th:NFA/MoO₃/Ag were fabricated to investigate photovoltaic performances. Multiple factors were taken into consideration when optimizing performance, including concentration and composition of photoactive layer materials, spin-casting rate, and the use of a processing additive, see Supporting Information. Best performances were achieved by using a weight ratio of 1:1.5 for PTB7-Th:NFA (total 18 mg mL⁻¹) with chlorobenzene (CB) as the main processing solvent and 1-chloronaphthalene (CN) as a solvent additive. The photovoltaic data of the best devices are listed in **Table 2**; optimization details are described in the Supporting information, see Figure S11 and

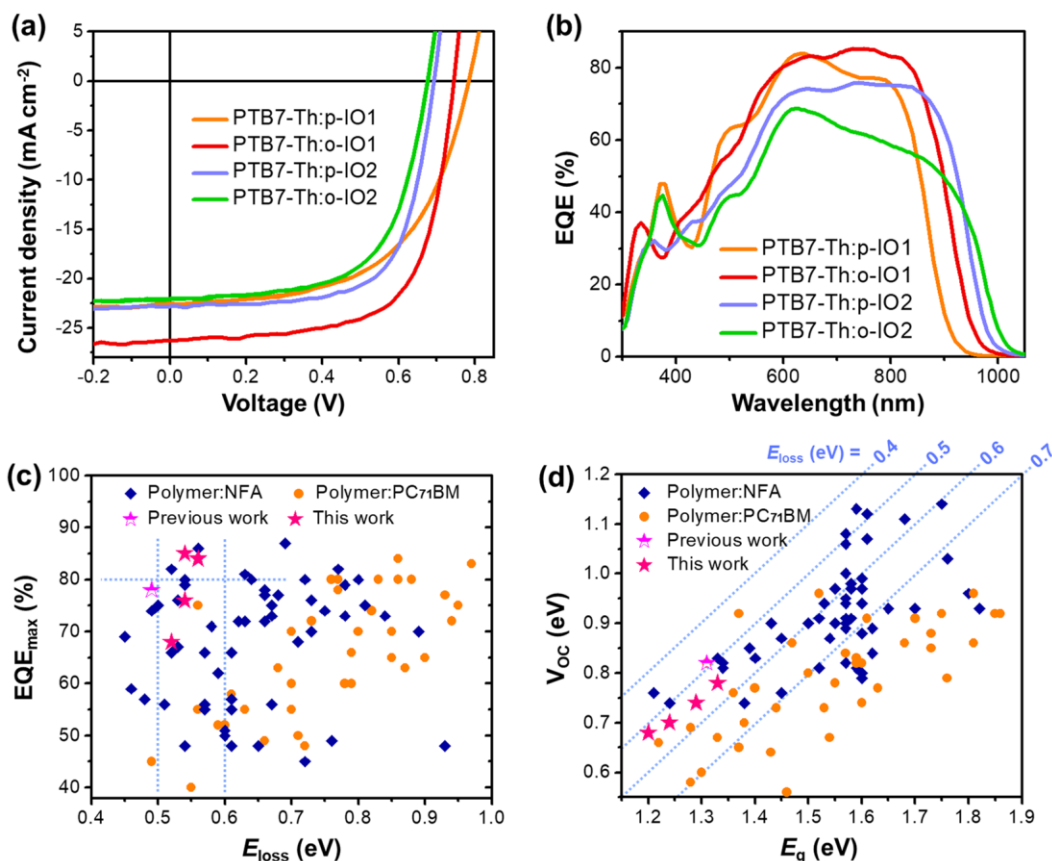


Figure 2. (a) J - V characteristics and (b) EQE spectra of the optimized solar cell devices under AM 1.5 G illumination at 100 mW cm^{-2} . Plots of (c) E_{loss} against EQE_{max} and (d) E_{g} against V_{oc} in various OSCs with fullerene or nonfullerene acceptors.

Table S1. **Figure 2a** presents current density–voltage (J - V) characteristics of the optimized solar cells prepared with CB:CN. Although the optimum CN ratio ranges from 2 vol% to 3 vol% (2 vol% for p-IO2, o-IO1, o-IO2 and 3 vol% for p-IO1, respectively), each molecule shows the similar PCEs within the conditions (Table S1). Optimized devices with p-IO1, o-IO1, p-IO2, and o-IO2 showed maximum PCEs (PCE_{max}) of 10.8%, 13.1%, 10.8%, and 9.3% with J_{sc} values of 22.3 mA cm^{-2} , 26.3 mA cm^{-2} , 23.0 mA cm^{-2} , and 21.8 mA cm^{-2} , respectively. Devices with p-IO1, o-IO1, p-IO2, and o-IO2 show V_{oc} values of 0.78 V, 0.74 V,

0.70 V, and 0.68 V, respectively, which follow expectations anticipated by examination of the energy differences between the LUMO of NFAs and the HOMO of PTB7-Th in Figure S10.

From the external quantum efficiencies (EQEs) of solar cells provided in Figure 2b one observes that the devices exhibit broad photoresponses ranging from 300 nm to 1000 nm, but reach EQE values of $\sim 80\%$ in the NIR region, in accordance with the absorption profiles of the active layer components. The J_{sc} integrated from EQE curves agrees with the values obtained from the J - V curves. Being aware of the challenge to achieve high EQEs and

Table 2. Photovoltaic performances of OSCs based on PTB7-Th and four NFAs measured under simulated 100 mW cm^{-2} AM 1.5G illumination.

Device ^a	V_{oc} (V)	J_{sc} (mA cm^{-2})	Cal. J_{sc} (mA cm^{-2}) ^b	FF	PCE_{max} (ave) (%) ^c	E_{loss} (eV)
PTB7-Th:p-IO1	0.78 (0.772 ± 0.004)	22.3 (22.19 ± 1.38)	21.9	0.62 (0.61 ± 0.03)	10.8 (10.34 ± 0.35)	0.56
PTB7-Th:o-IO1	0.74 (0.745 ± 0.004)	26.3 (25.37 ± 1.12)	24.7	0.67 (0.66 ± 0.01)	13.1 (12.57 ± 0.44)	0.54
PTB7-Th:p-IO2	0.70 (0.706 ± 0.010)	23.0 (21.99 ± 0.86)	22.6	0.67 (0.66 ± 0.01)	10.8 (10.24 ± 0.38)	0.54
PTB7-Th:o-IO2	0.68 (0.678 ± 0.004)	21.8 (21.28 ± 0.59)	20.0	0.63 (0.64 ± 0.02)	9.3 (9.14 ± 0.17)	0.52

^aPTB7-Th:acceptor blend ratios are 1:1.5 (w/w). 2–3 vol% CN was used as a processing solvent additive. ^bCalculated by integrating the EQE spectra. ^cThe average PCE values were obtained from over 12 devices.

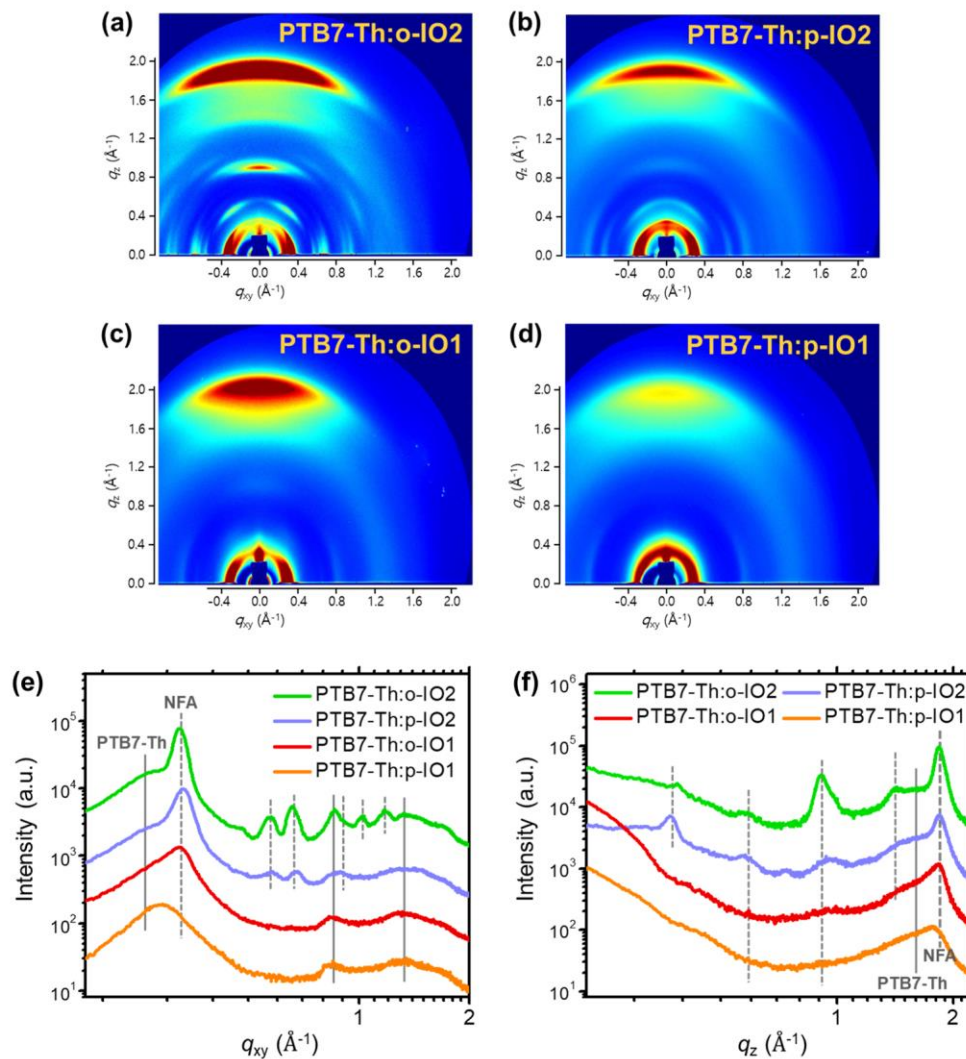


Figure 3. 2D GIWAXS images of (a) PTB7-Th:o-IO2, (b) PTB7-Th:p-IO2, (c) PTB7-Th:o-IO1, and (d) PTB7-Th:p-IO1 blend films. (e) In-plane and (f) out-of-plane line-cut profiles; solid lines and dotted lines indicate PTB7-Th and NFAs, respectively.

high V_{OC} simultaneously in NIR OSCs, we provide in Figure 2c a plot of $E_{QE_{max}}$ vs. E_{loss} using values reported in the literature (see Supporting Information).

State-of-the-art nonfullerene solar cells have achieved E_{loss} in the range of 0.5–0.6 eV with high EQEs (>70%), whereas most devices with PC₇₁BM exhibit E_{loss} values larger than ~0.7 eV (Figure 2c).^{45–48} We demonstrated that low energy loss of 0.49 eV and high $E_{QE_{max}}$ of 78% can be achieved simultaneously in a previous study.²² In this work, the E_{loss} of the optimized devices is ranging from 0.52 eV to 0.56 eV. It should be noted that the PTB7-Th:o-IO1 device exhibits an E_{loss} as low as 0.54 eV and $E_{QE_{max}}$ of 85% with EQE responses over 80% from 700 nm to 840 nm. This indicates that an excellent compromise between exciton dissociation/charge transfer and voltage loss was attained in the PTB7-Th:o-IO1 device, thus leading to a PCE of 13.1% with a J_{SC} of 26.3 mA·cm⁻² and a V_{OC} of 0.74 V. Figure 2d summarizes the correlation of eV_{OC} with E_g^{opt} using literature values. The majority of the devices exhibit E_{loss} of over 0.6 eV and only a few

cases with UNBG properties ($E_g^{opt} \leq 1.3$ eV) have been demonstrated. We have thus successfully developed UNBG-NFAs, enabling low E_{loss} NIR organic solar cells.

To obtain insight into the self-assembly of the BHJ components, grazing incidence wide-angle X-ray scattering (GIWAXS) was employed on films of the pure components and blends. Single component, p-IO1, o-IO1, p-IO2, and o-IO2, thin films processed with CB were first measured. From the 2D GIWAXS patterns (see Figure S12 in Supporting Information), one observes that the octyl-substituted o-IO1 and o-IO2 crystallites exhibit a preferential edge-on orientation relative to the substrate (Figures S6a and S6b), whereas the hexylphenyl-substituted p-IO2 orients face-on (Figures S6d). There is a larger number of diffraction peaks with o-IO2 compared to o-IO1. This is probably because o-IO2 with its symmetrical configuration has a higher tendency to crystallize in highly ordered domains, at least relative to the asymmetrical o-IO1.^{32,49,50} A similar tendency in crystallization for the symmetric vs. asymmetric structures can be observed for

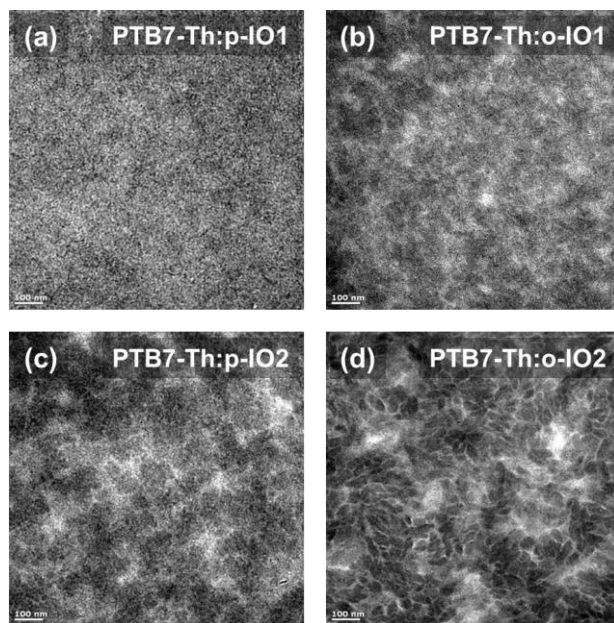


Figure 4. TEM images of (a) PTB7-Th:p-IO1, (b) PTB7-Th:o-IO1, (c) PTB7-Th:p-IO2, and (d) PTB7-Th:o-IO2 blend films processed with CB:CN.

p-IO2 and p-IO1. The p-IO1 film exhibits the weakest crystallization tendency among the four components in this study, probably as a result of the combination of the bulky alkylphenyl side chains and the asymmetrical configuration. Processing with CN additive encourages the four NFA molecules to be organized with face-on orientations. Clear diffraction peaks along the out-of-plane direction were observed for p-IO1, o-IO1, p-IO2, and o-IO2 with π - π stacking distances of 3.44 Å, 3.42 Å, 3.41 Å, and 3.40 Å, respectively. The slight contraction of packing distance is in accordance with the general crystallization features mentioned above.

The 2D GIWAXS images of the PTB7-Th:NFA blends processed with CN are shown in **Figure 3**. The crystallization propensity and molecular orientation of the blends with four NFAs follow the trends observed in the neat NFA films processed with CB:CN. The intensities of peaks around $q_{xy} = 0.325 \text{ \AA}^{-1}$ and $q_z = 1.83 \text{ \AA}^{-1}$ assigned to the NFA lamella (d -spacing: 19.3 Å) and π - π stacking (d -spacing: 3.43 Å), respectively, became weaker from o-IO2 to p-IO2 to o-IO1 to p-IO1 (Figure 3e and 3f). Consequently, the PTB7-Th:o-IO2 blends are dominated by the diffraction features of o-IO2 crystallites, whereas p-IO1 in the blends are relatively featureless.

We also examined the CB:CN-processed PTB7-Th:NFA blend films by using transmission electron microscopy (TEM). From **Figure 4**, one observes that phase separation and domain size become larger as the crystallization propensity of the molecules increases according to the order p-IO1 < o-IO1 < p-IO2 < o-IO2. Smallest apparent phase separation was observed in the PTB7-Th:p-IO1 blend. PTB7-Th:o-IO1 retains well-mixed phases with a slight increase in domain size. This indicates that non-symmetrical molecules tend to favor intermixing with

PTB7-Th, thereby facilitating exciton dissociation. Highest degree of phase separation is observed in the PTB7-Th:o-IO2 films (Figure 4d). It is possible to assign the dark grain-shape aggregates to the o-IO2-rich phases by electron energy loss spectroscopy (EELS) because only NFA molecules contain nitrogen atoms (see Figure S13). The higher crystallization propensity of the o-IO2 molecules induced by symmetrical configuration⁴⁹ and linear octyl side chains^{51,52} leads to growth of larger aggregates growth. Photoluminescence (PL) quenching tests were carried out to investigate charge transfer efficiency (Figure S14). Since PTB7-Th (donor) and the NFAs lie in spectral regions with sufficiently distinct wavelengths, they can be individually excited (640 nm and 808 nm for PTB7-Th and acceptors, respectively). The PL quenching efficiency of PTB7-Th:p-IO1 film is highest, whereas that of PTB7-Th:o-IO2 film is lowest; PTB7-Th:o-IO1 and PTB7-Th:p-IO1 are in the middle of them. Despite a broader absorption spectrum, the EQE responses of PTB7-Th:o-IO2-based device in the NIR region were lower than those of the devices based on the other NFAs (Figure 2b). This we attribute to the decreased interfacial area in the PTB7-Th:o-IO2 blend, a less favorable situation for charge generation.

In summary, we successfully synthesized a series of A- π -D- π -A type UNBG-NFAs, featuring efficient NIR photovoltaic properties with low E_{loss} . Modulating ICT effect by side chain modification of UNBG-NFAs enables tailoring of bandgaps and energetics, so as to optimize the energy diagram with respect to polymer PTB7-Th and thus to achieve highest possible V_{oc} values. Combination of linear octyl-substitution and non-symmetrical configuration in o-IO1 yields ordered crystallites and formation of suitable BHJ morphology with PTB7-Th, leading to the large photocurrent generation of the devices. Notably, the efficiency over 13% is one of the highest PCEs for the devices featuring UNBG properties ($E_{\text{g}}^{\text{opt}} \leq 1.3 \text{ eV}$). The molecular design strategy described here has the potential to be applied in the design of other electron acceptor materials.

ASSOCIATED CONTENT

Supporting Information

The Supporting Information is available free of charge on the ACS Publications website at DOI: XXX.

Synthesis details; NMR and electrochemical characterization; solar cell device fabrication and characterization; and morphology characterization (PDF)

AUTHOR INFORMATION

Corresponding Author

*E-mail: bazan@chem.ucsb.edu

*E-mail: kwcho@postech.ac.kr

Author Contributions

J. Lee and S. Song contributed equally to this work.

Notes

Any additional relevant notes should be placed here.

ACKNOWLEDGMENT

The authors are grateful to the Department of the Navy, Office of Naval Research (Award No. N00014-14-1-0580), the Center for Advanced Soft Electronics under the Global Frontier Research Program of the Ministry of Science, ICT & Future Planning, Korea (Grant Code No. 2011-0031628), and the Mitsubishi Chemical Center for Advanced Materials (MC-CAM) for financial support. This research was supported by the Technology Development Program to Solve Climate Changes of the National Research Foundation (NRF) funded by the Ministry of Science, ICT & Future Planning (NRF-2016M1A2A2940914). The authors are grateful to Hyun Jin Park in National Institute for Nanotechnology, Korea for the transmission electron microscopy measurements. The authors thank to the Pohang Accelerator Laboratory for providing the synchrotron radiation sources at 9A beamline used in this study.

REFERENCES

- (1) Dong, H.; Zhu, H.; Meng, Q.; Gong, X.; Hu, W. Organic Photoresponse Materials and Devices. *Chem. Soc. Rev.* **2012**, *41*, 1754–1808.
- (2) Ying, L.; Huang, F.; Bazan, G. C. Regioregular Narrow-Bandgap-Conjugated Polymers for Plastic Electronics. *Nat. Commun.* **2017**, *8*, 14047.
- (3) Cheng, Y.-J.; Yang, S.-H.; Hsu, C.-S. Synthesis of Conjugated Polymers for Organic Solar Cell Applications. *Chem. Rev.* **2009**, *109*, 5868–5923.
- (4) Arias, A. C.; MacKenzie, J. D.; McCulloch, I.; Rivnay, J.; Salleo, A. Materials and Applications for Large Area Electronics: Solution-Based Approaches. *Chem. Rev.* **2010**, *110*, 3–24.
- (5) Dou, L.; Liu, Y.; Hong, Z.; Li, G.; Yang, Y. Low-Bandgap Near-IR Conjugated Polymers/Molecules for Organic Electronics. *Chem. Rev.* **2015**, *115*, 12633–12665.
- (6) Brus, V. V.; Lee, J.; Luginbuhl, B. R.; Ko, S.-J.; Bazan, G. C.; Nguyen, T.-Q. Solution-Processed Semitransparent Organic Photovoltaics: From Molecular Design to Device Performance. *Adv. Mater.* **2019**, *31*, 1900904.
- (7) Tai, Q.; Yan, F. Emerging Semitransparent Solar Cells: Materials and Device Design. *Adv. Mater.* **2017**, *29*, 1700192.
- (8) Traverse, C. J.; Pandey, R.; Barr, M. C.; Lunt, R. R. Emergence of Highly Transparent Photovoltaics for Distributed Applications. *Nat. Energy* **2017**, *2*, 849–860.
- (9) Emmott, C. J. M.; Röhr, J. A.; Campoy-Quiles, M.; Kirchartz, T.; Urbina, A.; Ekins-Daukes, N. J.; Nelson, J. Organic Photovoltaic Greenhouses: A Unique Application for Semi-Transparent PV?. *Energy Environ. Sci.* **2015**, *8*, 1317–1328.
- (10) García de Arquer, F. P.; Armin, A.; Meredith, P.; Sargent, E. H. Solution-Processed Semiconductors for next-Generation Photodetectors. *Nat. Rev. Mater.* **2017**, *2*, 16100.
- (11) Liu, X.; Lin, Y.; Liao, Y.; Wu, J.; Zheng, Y. Recent Advances in Organic Near-Infrared Photodiodes. *J. Mater. Chem. C* **2018**, *6*, 3499–3513.
- (12) Wu, Z.; Zhai, Y.; Kim, H.; Azoulay, J. D.; Ng, T. N. Emerging Design and Characterization Guidelines for Polymer-Based Infrared Photodetectors. *Acc. Chem. Res.* **2018**, *51*, 3144–3153.
- (13) Huang, Y.; Kramer, E. J.; Heeger, A. J.; Bazan, G. C. Bulk Heterojunction Solar Cells: Morphology and Performance Relationships. *Chem. Rev.* **2014**, *114*, 7006–7043.
- (14) Yu, G.; Gao, J.; Hummelen, J. C.; Wudl, F.; Heeger, A. J. Polymer Photovoltaic Cells: Enhanced Efficiencies via a Network of Internal Donor-Acceptor Heterojunctions. *Science* **1995**, *270*, 1789–1791.
- (15) Lee, H.; Park, C.; Sin, D. H.; Park, J. H.; Cho, K. Recent Advances in Morphology Optimization for Organic Photovoltaics. *Adv. Mater.* **2018**, *30*, 1800453.
- (16) Nuzzo, D. D.; Wetzelaer, G.-J. A. H.; Bouwer, R. K. M.; Gevaerts, V. S.; Meskers, S. C. J.; Hummelen, J. C.; Blom, P. W. M.; Janssen, R. A. J. Simultaneous Open-Circuit Voltage Enhancement and Short-Circuit Current Loss in Polymer: Fullerene Solar Cells Correlated by Reduced Quantum Efficiency for Photoinduced Electron Transfer. *Adv. Energy Mater.* **2013**, *3*, 85–94.
- (17) Mishra, A.; Keshtov, M. L.; Looser, A.; Singhal, R.; Stolte, M.; Würthner, F.; Bäuerle, P.; Sharma, G. D. Unprecedented Low Energy Losses in Organic Solar Cells with High External Quantum Efficiencies by Employing Non-Fullerene Electron Acceptors. *J. Mater. Chem. A* **2017**, *5*, 14887–14897.
- (18) Li, Y.; Zhong, L.; Gautam, B.; Bin, H.-J.; Lin, J.-D.; Wu, F.-P.; Zhang, Z.; Jiang, Z.-Q.; Zhang, Z.-G.; Gundogdu, K.; et al. A Near-Infrared Non-Fullerene Electron Acceptor for High Performance Polymer Solar Cells. *Energy Environ. Sci.* **2017**, *10*, 1610–1620.
- (19) Bakulin, A. A.; Rao, A.; Pavelyev, V. G.; van Loosdrecht, P. H. M.; Pshenichnikov, M. S.; Niedzialek, D.; Cornil, J.; Beljonne, D.; Friend, R. H. The Role of Driving Energy and Delocalized States for Charge Separation in Organic Semiconductors. *Science* **2012**, *335*, 1340–1344.
- (20) Sini, G.; Schubert, M.; Risko, C.; Roland, S.; Lee, O. P.; Chen, Z.; Richter, T. V.; Dolfen, D.; Coropceanu, V.; Ludwigs, S.; Scherf, U.; Facchetti, A.; Fréchet, J. M.; Neher, D. On the Molecular Origin of Charge Separation at the Donor-Acceptor Interface. *Adv. Energy Mater.* **2018**, *8*, 1702232.
- (21) Baran, D.; Kirchartz, T.; Wheeler, S.; Dimitrov, S.; Abdelsamie, M.; Gorman, J.; S. Ashraf, R.; Holliday, S.; Wadsworth, A.; Gasparini, N.; et al. Reduced Voltage Losses Yield 10% Efficient Fullerene Free Organic Solar Cells with >1 V Open Circuit Voltages. *Energy Environ. Sci.* **2016**, *9*, 3783–3793.
- (22) Lee, J.; Ko, S.-J.; Seifrid, M.; Lee, H.; McDowell, C.; Luginbuhl, B. R.; Karki, A.; Cho, K.; Nguyen, T.-Q.; Bazan, G. C. Design of Nonfullerene Acceptors with Near-Infrared Light Absorption Capabilities. *Adv. Energy Mater.* **2018**, *8*, 1801209.
- (23) Gelinas, S.; Rao, A.; Kumar, A.; Smith, S. L.; Chin, A. W.; Clark, J.; van der Poll, T. S.; Bazan, G. C.; Friend, R. H. Ultrafast Long-Range Charge Separation in Organic Semiconductor Photovoltaic Diodes. *Science* **2014**, *343*, 512–516.
- (24) Wang, W.; Yan, C.; Lau, T.-K.; Wang, J.; Liu, K.; Fan, Y.; Lu, X.; Zhan, X. Fused Hexacyclic Nonfullerene Acceptor with Strong Near-Infrared Absorption for Semitransparent Organic Solar Cells with 9.77% Efficiency. *Adv. Mater.* **2017**, *29*, 1701308.
- (25) Gao, W.; Liu, T.; Ming, R.; Luo, Z.; Wu, K.; Zhang, L.; Xin, J.; Xie, D.; Zhang, G.; Ma, W.; Yan, H.; Yang, C. Near-Infrared Small Molecule Acceptor Enabled High-Performance Nonfullerene Polymer Solar Cells with Over 13% Efficiency. *Adv. Funct. Mater.* **2018**, *28*, 1803128.
- (26) Dai, S.; Li, T.; Wang, W.; Xiao, Y.; Lau, T.-K.; Li, Z.; Liu, K.; Lu, X.; Zhan, X. Enhancing the Performance of Polymer Solar Cells via Core Engineering of NIR-Absorbing Electron Acceptors. *Adv. Mater.* **2018**, *30*, 1706571.
- (27) Hou, J.; Inganäs, O.; Friend, R. H.; Gao, F. Organic Solar Cells Based on Non-Fullerene Acceptors. *Nat. Mater.* **2018**, *17*, 119–128.
- (28) Cheng, P.; Li, G.; Zhan, X.; Yang, Y. Next-Generation Organic Photovoltaics Based on Non-Fullerene Acceptors. *Nat. Photonics* **2018**, *12*, 131.
- (29) Lin, Y.; Zhan, X. Oligomer Molecules for Efficient Organic Photovoltaics. *Acc. Chem. Res.* **2016**, *49*, 175–183.
- (30) Nielsen, C. B.; Holliday, S.; Chen, H.-Y.; Cryer, S. J.; McCulloch, I. Non-Fullerene Electron Acceptors for Use in Organic Solar Cells. *Acc. Chem. Res.* **2015**, *48*, 2803–2812.
- (31) Lee, J.; Ko, S.-J.; Seifrid, M.; Lee, H.; Luginbuhl, B. R.; Karki, A.; Ford, M.; Rosenthal, K.; Cho, K.; Nguyen, T.-Q.; et al. Bandgap Narrowing in Non-Fullerene Acceptors: Single Atom

Substitution Leads to High Optoelectronic Response Beyond 1000 Nm. *Adv. Energy Mater.* **2018**, *8*, 1801212.

(32) Lee, J.; Ko, S.-J.; Lee, H.; Huang, J.; Zhu, Z.; Seifrid, M.; Vollbrecht, J.; Brus, V. V.; Karki, A.; Wang, H.; et al. Side-Chain Engineering of Nonfullerene Acceptors for Near-Infrared Organic Photodetectors and Photovoltaics. *ACS Energy Lett.* **2019**, *4*, 1401–1409.

(33) Yao, H.; Cui, Y.; Yu, R.; Gao, B.; Zhang, H.; Hou, J. Design, Synthesis, and Photovoltaic Characterization of a Small Molecular Acceptor with an Ultra-Narrow Band Gap. *Angew. Chem. Int. Ed.* **2017**, *56*, 3045–3049.

(34) Yao, Z.; Liao, X.; Gao, K.; Lin, F.; Xu, X.; Shi, X.; Zuo, L.; Liu, F.; Chen, Y.; Jen, A. K.-Y. Dithienopicenocarbazole-Based Acceptors for Efficient Organic Solar Cells with Optoelectronic Response Over 1000 Nm and an Extremely Low Energy Loss. *J. Am. Chem. Soc.* **2018**, *140*, 2054–2057.

(35) Xiao, Z.; Jia, X.; Li, D.; Wang, S.; Geng, X.; Liu, F.; Chen, J.; Yang, S.; Russell, T. P.; Ding, L. 26 mA cm⁻²Jsc from Organic Solar Cells with a Low-Bandgap Nonfullerene Acceptor. *Sci. Bull.* **2017**, *62*, 1494–1496.

(36) Li, Y.; Lin, J.-D.; Che, X.; Qu, Y.; Liu, F.; Liao, L.-S.; Forrest, S. R. High Efficiency Near-Infrared and Semitransparent Non-Fullerene Acceptor Organic Photovoltaic Cells. *J. Am. Chem. Soc.* **2017**, *139*, 17114–17119.

(37) Yao, H.; Chen, Y.; Qin, Y.; Yu, R.; Cui, Y.; Yang, B.; Li, S.; Zhang, K.; Hou, J. Design and Synthesis of a Low Bandgap Small Molecule Acceptor for Efficient Polymer Solar Cells. *Adv. Mater.* **2016**, *28*, 8283–8287.

(38) Liu, Y.; Li, M.; Yang, J.; Xue, W.; Feng, S.; Song, J.; Tang, Z.; Ma, W.; Bo, Z. High-Efficiency As-Cast Organic Solar Cells Based on Acceptors with Steric Hindrance Induced Planar Terminal Group. *Adv. Energy Mater.* **2019**, *9*, 1901280.

(39) Wang, W.; Zhao, B.; Cong, Z.; Xie, Y.; Wu, H.; Liang, Q.; Liu, S.; Liu, F.; Gao, C.; Wu, H.; et al. Nonfullerene Polymer Solar Cells Based on a Main-Chain Twisted Low-Bandgap Acceptor with Power Conversion Efficiency of 13.2%. *ACS Energy Lett.* **2018**, *3*, 1499–1507.

(40) Bin, H.; Yang, Y.; Peng, Z.; Ye, L.; Yao, J.; Zhong, L.; Sun, C.; Gao, L.; Huang, H.; Li, X.; Qiu, B.; Xue, L.; Zhang, Z.-G.; Ade, H.; Li, Y. Effect of Alkylsilyl Side-Chain Structure on Photovoltaic Properties of Conjugated Polymer Donors. *Adv. Energy Mater.* **2018**, *8*, 1702324.

(41) Privado, M.; Seco, C. R.; Singhal, R.; Cruz, P. d. I.; Langa, F.; Sharma, G. D.; Palomares, E. Reduced Energy Offsets and Low Energy Losses Lead to Efficient (~10% at 1 sun) Ternary Organic Solar Cells. *ACS Energy Letters* **2018**, *3*, 2418–2424.

(42) Bin, H.; Zhang, Z.-G.; Gao, L.; Chen, S.; Zhong, L.; Xue, L.; Yang, C.; Li, Y. Non-Fullerene Polymer Solar Cells Based on Alkylthio and Fluorine Substituted 2D-Conjugated Polymers Reach 9.5% Efficiency. *J. Am. Chem. Soc.* **2016**, *138*, 4657–4664.

(43) Yao, H.; Cui, Y.; Qian, D.; Ponseca, Jr. C. S.; Honarfar, A.; Xu, Y.; Xin, J.; Chen, Z.; Hong, L.; Gao, B.; Yu, R.; Zu, Y.; Ma, W.; Chabera, P.; Pullerits, T.; Yartsev, A.; Gao, F.; Hou, J. 14.7% Efficiency Organic Photovoltaic Cells Enabled by Active Materials with a Large Electrostatic Potential Difference. *J. Am. Chem. Soc.* **2019**, *141*, 7743–7750.

(44) Liu, J.; Chen, S.; Qian, D.; Gautam, B.; Yang, G.; Zhao, J.; Bergqvist, J.; Zhang, F.; Ma, W.; Ade, H.; Inganäs, O.; Gundogdu, K.; Gao, F.; Yan, H. Fast Charge Separation in a Non-Fullerene Organic Solar Cell with a Small Driving Force. *Nat. Energy* **2016**, *1*, 16089.

(45) Bin, H.; Gao, L.; Zhang, Z.-G.; Yang, Y.; Zhang, Y.; Zhang, C.; Chen, S.; Xue, L.; Yang, C.; Xiao, M.; Li, Y. 11.4% Efficiency Non-Fullerene Polymer Solar Cells with Trialkylsilyl Substituted 2D-Conjugated Polymer as Donor. *Nat. Commun.* **2016**, *7*, 13651.

(46) Chen, S.; Wang, Y.; Zhang, L.; Zhao, J.; Chen, Y.; Zhu, D.; Yao, H.; Zhang, G.; Ma, W.; Friend, R. H.; Chow, P. C. Y.; Gao, F.; Yan, H. Efficient Nonfullerene Organic Solar Cells with Small Driving Forces for Both Hole and Electron Transfer. *Adv. Mater.* **2018**, *30*, 1804215.

(47) Wang, Y.; Qian, D.; Cui, Y.; Zhang, H.; Hou, J.; Vandewal, K.; Kirchartz, T.; Gao, F. Optical Gaps of Organic Solar Cells as a Reference for Comparing Voltage Losses. *Adv. Energy Mater.* **2018**, *8*, 1801352.

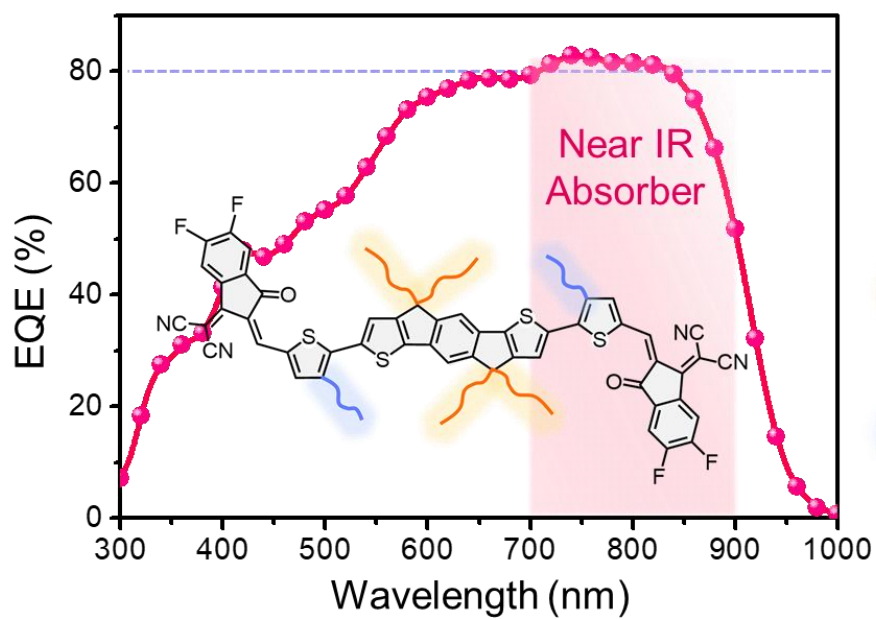
(48) Li, S.; Zhan, L.; Sun, C.; Zhu, H.; Zhou, G.; Yang, W.; Shi, M.; Li, C.-Z.; Hou, J.; Li, Y.; Chen, H. Highly Efficient Fullerene-Free Organic Solar Cells Operate at Near Zero Highest Occupied Molecular Orbital Offsets. *J. Am. Chem. Soc.* **2019**, *141*, 3073–3082.

(49) Li, C.; Fu, H.; Xia, T.; Sun, Y. Asymmetric Nonfullerene Small Molecule Acceptors for Organic Solar Cells. *Adv. Energy Mater.* **2019**, *9*, 1900999.

(50) Gao, W.; Zhang, M.; Liu, T.; Ming, R.; An, Q.; Wu, K.; Xie, D.; Luo, Z.; Zhong, C.; Liu, F.; et al. Asymmetrical Ladder-Type Donor-Induced Polar Small Molecule Acceptor to Promote Fill Factors Approaching 77% for High-Performance Nonfullerene Polymer Solar Cells. *Adv. Mater.* **2018**, *30*, 1800052.

(51) Fei, Z.; Eisner, F. D.; Jiao, X.; Azzouzi, M.; Röhr, J. A.; Han, Y.; Shahid, M.; Chesman, A. S. R.; Easton, C. D.; McNeill, C. R.; et al. An Alkylated Indacenodithieno[3,2-b]Thiophene-Based Nonfullerene Acceptor with High Crystallinity Exhibiting Single Junction Solar Cell Efficiencies Greater than 13% with Low Voltage Losses. *Adv. Mater.* **2018**, *30*, 1705209.

(52) Song, X.; Gasparini, N.; Nahid, M. M.; Chen, H.; Macphree, S. M.; Zhang, W.; Norman, V.; Zhu, C.; Bryant, D.; Ade, H.; McCulloch, I.; Baran, D. A Highly Crystalline Fused-Ring n-Type Small Molecule for Non-Fullerene Acceptor Based Organic Solar Cells and Field-Effect Transistors. *Adv. Funct. Mater.* **2018**, *28*, 1802895.



Side Chain Engineering

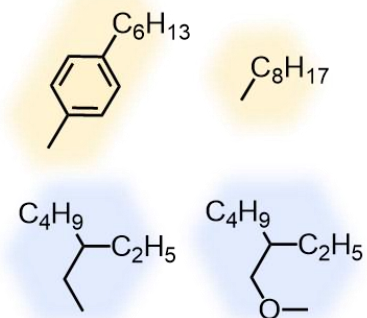


Table of Contents